


Spontaneous Article

Arsenate removal from aqueous solutions by Mg/Fe-LDH-modified biochar derived from apple tree residues

Mohammad Ali SHIRIAZAR¹, Ebrahim SEPEHR^{1*} , Ramin MALEKI², Habib KHODAVERDILOO¹, Farrokh ASADZADEH¹, Behnam DOVLATI¹ and Zed RENGEL^{3,4}

¹ Soil Science Department, Faculty of Agriculture, University of Urmia, SERO Road, PO Box 165, 5756151818, Urmia, Iran.

² Research Department of Chromatography, Iranian Academic Center for Education, Culture and Research (ACECR), Urmia Branch, Beheshti Street, PO Box 168, 5715944919, Urmia, Iran.

³ Soil Science and Plant Nutrition, UWA School of Agriculture and Environment, The University of Western Australia, 35 Stirling Highway, PERTH WA 6009, Australia.

⁴ Institute for Adriatic Crops and Karst Reclamation, Split, Croatia.

*Corresponding author. Email: e.sepehr@urmia.ac.ir

ABSTRACT: The development of non-toxic and inexpensive materials for arsenic removal is required due to water sources being polluted by arsenic in many countries around the world. The main aim of this study was to characterise the capacity and behaviour of Mg/Fe layered double hydroxides/biochar [Magnesium/Iron-Layered Double Hydroxide (Mg/Fe-LDH)] composite for arsenate adsorption from solution. Apple tree pruning residues were used to produce biochar at 500 °C under oxygen-limited atmosphere. Mg/Fe-LDH-biochar was synthesised using a spontaneous *in situ* co-precipitation method. Batch experiments were used for the assessment of the kinetics, isotherms, and the effects of initial solution pH (4, 6, 8, and 10), ionic strength (0.01, 0.1, and 0.2 mol L⁻¹), and co-occurring anions (carbonate and phosphate) on the arsenate removal. Scanning electron microscope images showed Mg/Fe-LDH were loaded on the biochar porous structure, and X-ray diffraction analysis affirmed the presence of crystalline LDH minerals in Mg/Fe-LDH-biochar. Surface modification of biochar by Mg/Fe-LDH increased the maximum arsenate adsorption capacity (3.6 mg g⁻¹) ten times compared to unmodified biochar (0.35 mg g⁻¹). Arsenate removal capacity increased from 4.2% to 54.2% with modification of biochar by Mg/Fe-based LDH. Kinetic studies indicated that >90% of Mg/Fe-LDH-biochar arsenate adsorption from a starting concentration of 10 mg L⁻¹ occurred in the first 120 min. Pseudo-second order and Langmuir models described well the kinetics and isotherm of arsenate adsorption by biochar and Mg/Fe-LDH-biochar. Mg/Fe-LDH-biochar showed maximum arsenate removal capacity at pH 6. Increasing solution ionic strength and the presence of phosphate and carbonate anions suppressed arsenate removal by Mg/Fe-LDH-biochar. In summary, surface modification of biochar using Mg/Fe-LDH produced a potentially more cost-effective, locally available, reusable, and non-toxic arsenic adsorbent for decontamination of surface- and groundwater.



KEY WORDS: adsorbents, arsenic, contamination, isotherm, maximum capacity.

Arsenic, as a metalloid, has detrimental effects on human health and is categorised as a class 1 carcinogenic agent (Singh *et al.* 2015; He *et al.* 2018). Chronic exposure to arsenic (arsenic-contaminated water, air, and food) can cause immunological and neurological complications, as well as cancers including those of lung and skin (Sadeghi *et al.* 2017).

Natural processes such as mineral weathering are the global-scale causes of arsenic release into the environment, especially groundwater; these processes are accelerated by human activities such as mining (Elwakeel & Guibal 2015). Arsenate (HAsO₄²⁻, H₂AsO₄⁻) and arsenite (H₃AsO₃, H₂AsO₃⁻) are the most important inorganic species of arsenic in aqueous systems in natural conditions. Arsenate is the stable species in aerobic

conditions, whereas arsenite is the dominant form of inorganic arsenic in anoxic media (Manirethan *et al.* 2020).

The range of arsenic concentration in natural waters is typically 0.0005 to 5 mg L⁻¹ (Singh *et al.* 2015). In areas where groundwater is the main drinking water source, the risk of arsenic poisoning to humans is serious. The maximum permissible concentration of arsenic in drinking water established by the World Health Organization (WHO) is 0.01 mg L⁻¹ (WHO 2017). It is estimated that arsenic-contaminated drinking water affects more than 150 million people around the world (Singh *et al.* 2015), including some areas of Iran where arsenic contamination of water resources has caused health problems (Sadeghi *et al.* 2017). Hence, it is essential to provide arsenic-free

groundwater/drinking water by simple and inexpensive methods (Shabbir *et al.* 2020), especially considering the rural regions in developing countries.

Comparing the advantages and disadvantages of the arsenic removal methods, adsorption processes are considered an effective method for removing arsenic from water because they are simple and inexpensive, produce minimal toxic waste, and are useful for water-based media or low levels of pollutants that need to be removed quickly. Recently, researchers have focused on finding new adsorbents that would be low-cost, with good mechanical and chemical resistance, widely available, easy to manufacture, and with high adsorption capacity. It is unrealistic to expect all the above-mentioned properties in an adsorbent, but most of these properties are necessary for a good adsorbent. In the past decades, materials such as hematite, magnetite, goethite (Giménez *et al.* 2007), iron–zirconium (Fe–Zr) binary oxide (Ren *et al.* 2011), and composites such as chitosan-encapsulated copper hydroxide (Cu(OH)₂) and copper oxide (CuO) (Elwakeel & Guibal 2015) have been used for arsenic removal from aqueous solutions.

Biochar is a carbon-rich and relatively stable material produced by thermal pyrolysis of solid agro/industrial wastes under limited oxygen conditions. The cost of producing biochar is estimated to be US\$0.066 per kilogram, which is about 3–6% of the price of other commercial carbon-based adsorbents (Yoder *et al.* 2011). Biochar surface area is affected by the pyrolysis temperature, whereby the high-temperature-derived biochars have large surface area (Vithanage *et al.* 2017).

Biochar is considered as a good sorbent for many heavy metals due to its large surface area, and elevated capacity for cation exchange due to organic functional groups, but the biochar capacity to remove (oxy)anionic pollutants (such as arsenate) from aquatic environments is low (Lin *et al.* 2017) due to the negatively charged surfaces. Hence, modifications of biochar to increase the anion sorption capacity are needed to improve removal of pollutants, done mainly by creating new functional groups (active sorption sites). Biochar modifications using iron chloride (He *et al.* 2018), iron oxide (Fe₃O₄) nanoparticles (Alchouron *et al.* 2020), and iron-manganese (Fe–Mn) oxides (Lin *et al.* 2017) have been reported for arsenate decontamination of water, but further work is needed to develop low-cost and simple techniques to modify biochar with non-toxic materials that enhance the arsenate-sorption properties of biochar.

In the last few decades, anionic clays, known as layered double hydroxides (LDHs) due to their unique properties (high anion exchange capacity and large surface area), have been used to adsorb oxyanions from aqueous solutions (Dias & Fontes 2020). LDHs have brucite-like (magnesium hydroxide) structures where magnesium (Mg²⁺) is coordinated octahedrally by six hydroxyl (OH[−]) ions. Substitution of some divalent metal cations with trivalent metal cations leads to positive charge appearing on the brucite-like layers; these charges are commonly balanced by inorganic anions (oxyanions and halides) in the interlayer spaces (Cui *et al.* 2019).

The use of powdered LDHs as adsorbents has limitations such as low dispersion in the solution and blockage of filters that causes a pressure drop in the fixed-bed systems (Goh *et al.* 2008). On the other hand, arsenate adsorption capacity of biochar is relatively low, but biochar can be utilised as a support material for powdered LDHs because of its porous structure, large surface area, and chemical stability. Hence, biochar modification using LDH to fabricate mineral-organic adsorbents could provide a novel route to eliminate the intrinsic limitations of biochar and LDH regarding arsenate decontamination of water. In the literature, application of LDH-modified biochar for decontamination of pollutants such as nitrate (Xue *et al.* 2016), methylene blue (Meili *et al.* 2019), and phosphate

(Zhang *et al.* 2013a, 2013b) has been documented. However, modification of biochar by Magnesium/Iron-Layered Double Hydroxide (Mg/Fe-LDH) with chloride (Cl[−]) as interspersed anion for arsenate removal has not been recognised. The objectives of the present study were to (1) characterise biochar and Mg/Fe-LDH-biochar using X-ray diffraction (XRD) and scanning electron microscopy (SEM); (2) analyse arsenate adsorption kinetics and isotherms using biochar and Mg/Fe-LDH-biochar; and (3) assess the effects of solution initial pH, ionic strength (IS), and co-occurring anions (carbonate and phosphate) on arsenate adsorption on Mg/Fe-LDH-biochar.

1. Materials and methods

1.1. Chemicals

Analytical-grade sodium arsenate dibasic heptahydrate (Na₂HAsO₄·7H₂O), concentrated hydrochloric acid (HCl), sodium carbonate (Na₂CO₃), potassium dihydrogen phosphate (KH₂PO₄), magnesium chloride hexahydrate (MgCl₂·6H₂O), sodium hydroxide (NaOH), iron(III) chloride hexahydrate (FeCl₃·6H₂O), and sodium nitrate (NaNO₃) were provided by Sigma-Aldrich and Merck Chemical Co. All analytical-grade reagents or chemicals were used in all adsorption experiments without further purification. Deionised (DI) water was used to rinse and clean the samples, and to prepare all experimental solutions.

1.2. Adsorbent preparation

In this study, apple tree pruning residues were used as biomass to produce biochar. Biomass feedstock was dried at 110 °C for 24 h, then milled and sieved through 2 mm. The pyrolysis of powder was done in a reactor at 500 °C under oxygen-limited conditions for 2 h. Mg/Fe-LDH-biochar was synthesised via the spontaneous co-precipitation method by adding biochar to a mixed solution of Mg and Fe metals at high pH according to the literature (Xue *et al.* 2016). To prepare Mg/Fe-LDH-biochar, 10 g of raw biochar was mixed with 100 mL of Mg/Fe solution at a molar ratio of 2 (Mg + Fe = 0.06 mole) prepared using MgCl₂·6H₂O and FeCl₃·6H₂O. The pH of suspension was adjusted to 10 by the addition of NaOH; the suspension was heated (70 °C) for 72 h, and the composite was rinsed in DI and dried at 70 °C for 24 h before use.

1.3. Characterisation of adsorbents

SEM images were recorded using a SERON Technologies Inc. microscope (Model: AIS 2100) operating at an accelerating voltage of 20 keV. Non-modified biochar and Mg/Fe-LDH-biochar were also analysed by an X-ray diffractometer (Shimadzu-6000) equipped with a Cu-K α radiation source; scanning was done at 2° per min. Carbon, hydrogen, and nitrogen contents of the adsorbents were determined by an elemental analyser (ECS 4010 CHNSO Analyzer). Cation exchange capacity of the adsorbents was measured using a modified ammonium-acetate method (Gaskin *et al.* 2008). The electrical conductivity (EC) and pH were measured in a 1:20 (adsorbent:water) suspension after shaking for 1 h (Singh *et al.* 2010). Specific surface area was analysed according to Sears (1956). The point of zero charge (pH_{pzc}) of biochar and Mg/Fe-LDH-biochar was determined using the pH drift method (Niasar *et al.* 2016). Briefly, 50 mL of 0.1 mol L^{−1} sodium chloride at different pHs (ranging from 2 to 12) was added to 0.15 g of adsorbents, and then mixtures were shaken at room temperature (19 ± 1 °C) at a rate of 170 rpm for 32 h. Finally, the pH of solution was determined and plotted against the initial pH, and the intersection point of pH_{final} vs pH_{initial} was considered as the pH_{pzc} of the adsorbents.

1.4. Kinetics

Na₂HAsO₄·7H₂O (4.16 g) was used for preparation of 1000 mg L⁻¹ of arsenate stock solution. In this work, 0.01 mol L⁻¹ NaNO₃ was used as a background solution. For the kinetic batch experiments, 30 mg of selected adsorbents (unmodified biochar or Mg/Fe-LDH-biochar) was mixed with 40 mL of 10 mg L⁻¹ arsenate solution (pH = 7 ± 0.1, IS = 0.01 mol L⁻¹) and shaken at 100 rpm at room temperature (19 ± 1 °C) for specific time intervals. All suspensions were filtered (0.45 μm), and the filtrate was analysed for arsenic concentration.

The arsenate adsorbed on the solid phase (q_e , mg g⁻¹) and arsenate removal efficiency (RE: %) by adsorbents were obtained from Eq. 1 and Eq. 2 (Shabbir *et al.* 2020), respectively:

$$q_e = \frac{(C_0 - C_e) \times V}{M} \quad (1)$$

$$\% RE = \frac{(C_0 - C_e) \times 100}{C_0} \quad (2)$$

where C_0 and C_e are, respectively, the initial and equilibrium arsenate concentrations in solution (mg L⁻¹), V is the arsenate solution volume (L), and M is the adsorbent weight (g).

The data on arsenate adsorption kinetics were fitted to several kinetics models such as pseudo-first order (PFO), pseudo-second order (PSO), Elovich, and fractional power. The non-linear mathematical form of PFO model is given in Eq. 3 (Tan & Hameed 2017):

$$q_t = q_e(1 - e^{-k_1 t}) \quad (3)$$

where q_e (mg g⁻¹) is the amount of sorbed arsenate at equilibrium, q_t (mg g⁻¹) is the quantity of sorbed arsenate at time t (min), and k_1 (min⁻¹) is the constant of PFO model that is dependent on the process conditions.

The non-linear form of PSO model is indicated by Eq. 4 (Tan & Hameed 2017):

$$q_t = \frac{k_2 q_e^2 t}{1 + k_2 q_e t} \quad (4)$$

where k_2 (g mg⁻¹ min⁻¹) is the constant of the PSO model.

The fractional power model is expressed by Eq. 5 (Inyinbor *et al.* 2016):

$$q_t = k_{FP} t^v \quad (5)$$

where k_{FP} (mg g⁻¹) and v (min⁻¹) are the fractional power model rate constants, with v being normally less than 1 when experimental data fit the model well.

The non-linear form of the Elovich kinetic model is depicted by Eq. 6 (Tan & Hameed 2017):

$$q_t = \frac{1}{\beta} \ln(1 + \alpha \beta t) \quad (6)$$

where α (mg g⁻¹ min⁻¹) is the initial adsorption rate, and β (g mg⁻¹) is the desorption constant.

1.5. Isotherms

Adsorption isotherms of arsenate by Mg/Fe-LDH-biochar and unmodified biochar were produced by mixing 30 mg of Mg/Fe-LDH-biochar or biochar with 40 mL of different concentrations (ranging from 1 to 25 mg L⁻¹) of arsenate solutions (pH = 7 ± 0.1, IS = 0.01 mol L⁻¹) in polypropylene Falcon tubes. The tubes were shaken at 100 rpm at room temperature (19 ± 1 °C) for 16 h. The samples were filtered (0.45 μm) to determine arsenate concentration in the residual solution; then, Eq. 1 was used to calculate arsenate sorbed on the solid phase.

Isotherm data were simulated by the Langmuir, Freundlich, Temkin, and Dubinin–Radushkevich (D–R) models. The non-linear Langmuir model is shown in Eq. 7 (Foo & Hameed 2010):

$$q_e = \frac{q_{max} K_L C_e}{1 + K_L C_e} \quad (7)$$

where q_e (mg g⁻¹) is sorbed arsenate at the equilibrium arsenate concentration (C_e , mg L⁻¹). K_L (L mg⁻¹) and q_{max} (mg g⁻¹) are the constant of Langmuir model and the maximum capacity of adsorption, respectively.

The Freundlich model assumes multilayers of adsorbate on a heterogeneous surface of adsorbent, and is depicted in Eq. 8 (Foo & Hameed 2010):

$$q_e = K_F C_e^{1/n} \quad (8)$$

where K_F is the constant of Freundlich isotherm model, an indicator of the adsorption capacity [(mg g⁻¹)(Lmg⁻¹)^{-1/n}], and n is the dimensionless parameter referred to as a heterogeneity factor.

The Temkin non-linear mathematical form is depicted in Eq. 9 (Inyinbor *et al.* 2016):

$$q_e = B_T \ln(A_T C_e) \quad (9)$$

where A_T (L g⁻¹) and B_T are the Temkin isotherm model constants, whereby B_T is related to the heat of adsorption and is defined by Eq. 10:

$$B_T = \frac{RT}{b_T} \quad (10)$$

where b_T (J mol⁻¹) is the constant of Temkin model, T is the temperature (292 K), and R is the gas constant (8.314 J mol⁻¹ K⁻¹).

The D–R model is empirical; it does not assume a homogeneous surface and is commonly used to separate the physical and chemical adsorption of adsorbates on adsorbents (Foo & Hameed 2010). The mathematical form of the D–R model is given in Eq. 11:

$$q_e = q_s \exp(-k_{DR} \varepsilon^2) \quad (11)$$

where q_s is the saturation capacity (mg g⁻¹), and k_{DR} is the D–R model constant (mol² kJ⁻²). ε is the constant of the D–R model that can be represented by Eq. 12:

$$\varepsilon = RT \ln \left(1 + \frac{1}{C_e} \right) \quad (12)$$

1.6. Initial pH and IS

The impact of pH on arsenate removal by Mg/Fe-LDH-biochar was assessed at pH ranging from 4 to 10. Briefly, 40 mL of 10 mg L⁻¹ arsenate solution (IS = 0.01 mol L⁻¹) was mixed with 30 mg of Mg/Fe-LDH-biochar, and the initial pH was adjusted to 4, 6, 8, and 10 by 0.1 mol L⁻¹ NaOH and 0.1 mol L⁻¹ HCl. For characterising the IS influence, experiments were done by mixing 30 mg Mg/Fe-LDH-biochar with 40 mL of 10 mg L⁻¹ arsenic solution (pH = 7 ± 0.1) in polypropylene Falcon tubes. The background solution IS was adjusted by NaNO₃ (ranging from 0.01 to 0.2 mol L⁻¹). Samples were shaken at room temperature (19 ± 1 °C) at the rate of 100 rpm for 16 h, followed by filtration through 0.45-μm membrane, and filtrates were kept for arsenate analysis.

The central composite design, as the standard response surface method (RSM), was selected for factors that had large influence on arsenate adsorption on Mg/Fe-LDH-biochar. In this design, pH (4 to 10) and IS of background solution (0.01 to 0.2 mol L⁻¹) were independent factors. The combined effects of these two factors on arsenate removal from solution were assessed in 13 sets of samples.

1.7. Co-occurring ions

The influence of common competing anions on the arsenate removal was evaluated using 1 mmol L⁻¹ carbonate and phosphate solutions. Briefly, 30 mg of Mg/Fe-LDH-biochar was mixed with 40 mL of 10 mg L⁻¹ arsenate containing 1 mmol L⁻¹ of phosphate or carbonate (pH = 7 ± 0.1, IS = 0.01 mol L⁻¹) and shaken at 100 rpm at room temperature (19 ± 10 °C) for 16 h. Finally, suspensions were filtered (0.45 µm) to analyse arsenic concentration.

1.8. Generation cycles

Adsorbent regeneration is one of the important considerations for long-term use in water decontamination. For regeneration of spent Mg/Fe-LDH-biochar, 0.1 mol L⁻¹ NaOH was used as the desorption agent in a batch system. After arsenate adsorption (30 mg of adsorbent mixed with 40 mL of 100 µg L⁻¹ solution of arsenate, shaken at 100 rpm at room temperature (19 ± 10 °C) for 16 h), the arsenate-laden Mg/Fe-LDH-biochar was filtered (0.45 µm) and rinsed with DI water thrice to remove residual arsenate. Then, spent Mg/Fe-LDH-biochar was mixed with 100 mL of 0.1 mol L⁻¹ NaOH, stirred at the rate of 100 rpm for 12 h to desorb arsenate, and then filtered through 0.45-µm membrane. Finally, the arsenate adsorption–desorption steps were repeated for five cycles.

1.9. Arsenate determination in solution

The arsenic concentration in the solution samples was measured using a Perkin Elmer AAnalyst 800 graphite furnace atomic absorption spectrometer.

1.10. Statistical analyses

Different kinetic and isotherm models were fitted using non-linear regression using the method of least squares. Excel-solver software was used for statistical analyses and curve fitting. The coefficient of determination (R^2 ; Eq. 12) and the standard error (SE; Eq. 13) were used for the statistical analysis of the kinetics and isotherm models for comparisons.

$$R^2 = \frac{\sum (q_{e,cal} - \overline{q_{e,exp}})^2}{\sum (q_{e,cal} - \overline{q_{e,exp}})^2 + \sum (q_{e,cal} - q_{e,exp})^2} \quad (13)$$

$$SE = \sqrt{\frac{1}{n-2} \sum_{i=1}^n (q_{e,cal} - q_{e,exp})^2} \quad (14)$$

where $q_{e,exp}$, $q_{e,cal}$, and n are the measured adsorbed arsenate, the calculated adsorbed arsenate using models, and the number of experimental data points, respectively. Minitab 17 software was used for the RSM design and the graphical illustration of the interaction between initial pH and background solution IS.

2. Results and discussion

2.1. Adsorbent morphological structure

The microstructures of adsorbents (unmodified biochar and Mg/Fe-LDH-biochar) were characterised by SEM (Fig. 1). The unmodified biochar SEM images showed the porous and non-uniform structure. Clearly, the Mg/Fe-LDH-biochar was rougher than unmodified biochar and mainly comprised two-phase, which included raw biochar and micro-sized Mg/Fe-LDH particles, as shown in the yellow circles in Fig. 1. The XRD diffractogram of unmodified biochar and Mg/Fe-LDH-biochar, using the 2-theta range of 2–65°, is shown in Figure 2. The presence of sharp and symmetrical peaks commonly demonstrate strong crystallinity of the minerals in the samples (Nhat Ha *et al.* 2016). The XRD analysis of unmodified biochar revealed the crystalline form of calcite at $2\theta = 29.44^\circ$,

44.55°, and 23.28° corresponding to d spacings of 3.03 Å, 2.05 Å, and 3.8 Å, respectively. These peaks almost completely disappeared after modification by Mg/Fe-LDH, which may be ascribed to the reduced amount of calcite after the modification. The presence of Mg/Fe-LDH crystals on the biochar surface was confirmed by the presence of LDH characteristic diffraction peaks in the XRD diffractogram of Mg/Fe-LDH-biochar, since these peaks were absent in unmodified biochar. The dominant peaks in XRD pattern of Mg/Fe-LDH-biochar were at $2\theta = 10.55^\circ$, 22.054° , and 33.41° , which corresponded well with the typical XRD patterns of LDHs reported in other studies (Goh *et al.* 2008; Hudcová *et al.* 2019).

The specific surface area of the unmodified biochar was 266 m² g⁻¹ (supplementary Table 1 available at <https://doi.org/10.1017/S1755691022000019>). Biochars with a large surface area and porous structure are suitable for removal of contaminants from water. The specific surface area of the Mg/Fe-LDH-modified biochar was 50 m² g⁻¹. The low specific surface area of the Mg/Fe-LDH-biochar hybrid than the raw biochar indicates that much of the biochar pore space was filled with Mg/Fe-LDH flakes during the co-precipitation, which was confirmed by the SEM images (Fig. 1). The pH decreased by 10.5% from 9.5 in the pristine biochar to 8.5 in Mg/Fe-LDH-biochar after loading with Mg/Fe-LDH, whereas EC was increased from 0.12 to 0.53 dS m⁻¹. The elemental composition of unmodified biochar and Mg/Fe-LDH-biochar was obtained from CHNSO Analyzer (supplementary Table 1). Compared with pristine biochar, the carbon (C), hydrogen (H), and nitrogen (N) contents of Mg/Fe-LDH-biochar dropped after Mg/Fe-LDH introduction, whereas the inverse trend was observed for the Mg and Fe contents.

2.2. pH_{pzc} of adsorbents

The pH_{pzc} is considered to be the most important factor that affects removal of metal(loid)s using adsorbents of variable charge. The pH_{pzc} values obtained for biochar and Mg/Fe-LDH-biochar were 9 and 10, respectively (supplementary Fig. 1). The high pH_{pzc} value of biochar could be due to the formation of oxides, carbonates, and aromatic components during pyrolysis at high temperature (Karunanayake *et al.* 2019). pH_{pzc} values of 10 have been reported for Mg/Fe-LDH (Hudcová *et al.* 2019) and of 8.46 for biochar derived from pulp and paper sludge (Chaukura *et al.* 2017); these reported values were in line with the values measured in the present study.

2.3. Arsenate RE

Application of non-modified biochar and Mg/Fe-LDH-biochar for arsenate removal from solution (pH = 7, IS = 0.01 mol L⁻¹) demonstrated that arsenate RE from solution was significantly higher for Mg/Fe-LDH-biochar compared to non-modified biochar at various initial arsenate concentrations (ranging from ≈1 to 25 mg L⁻¹; Table 1). Arsenate removal rate increased from 4.2% to 54.2% (arsenate initial concentration ≈1 mg L⁻¹) with modification of biochar using Mg/Fe-LDH. As the arsenate concentration in solution increased, the RE of adsorbents decreased, especially in the case of Mg/Fe-LDH-biochar.

Generally, electrostatic interactions and complexation are the important mechanisms for arsenate adsorption by biochar. The arsenate speciation as a function of pH for this study was simulated by Visual MINTEQ software. Under the experimental conditions (pH = 7), HAsO₄²⁻ and H₂AsO₄⁻ were likely to be the predominant arsenate species (supplementary Fig. 2). As the pH_{pzc} of biochar was above 7 (9; Section 2.2), some of the functional groups of the biochar would have been positively charged. Consequently, the anionic species of arsenate may interact with the positively charged functional groups on the biochar surface via electrostatic forces. Li *et al.* (2017) stated the complexation

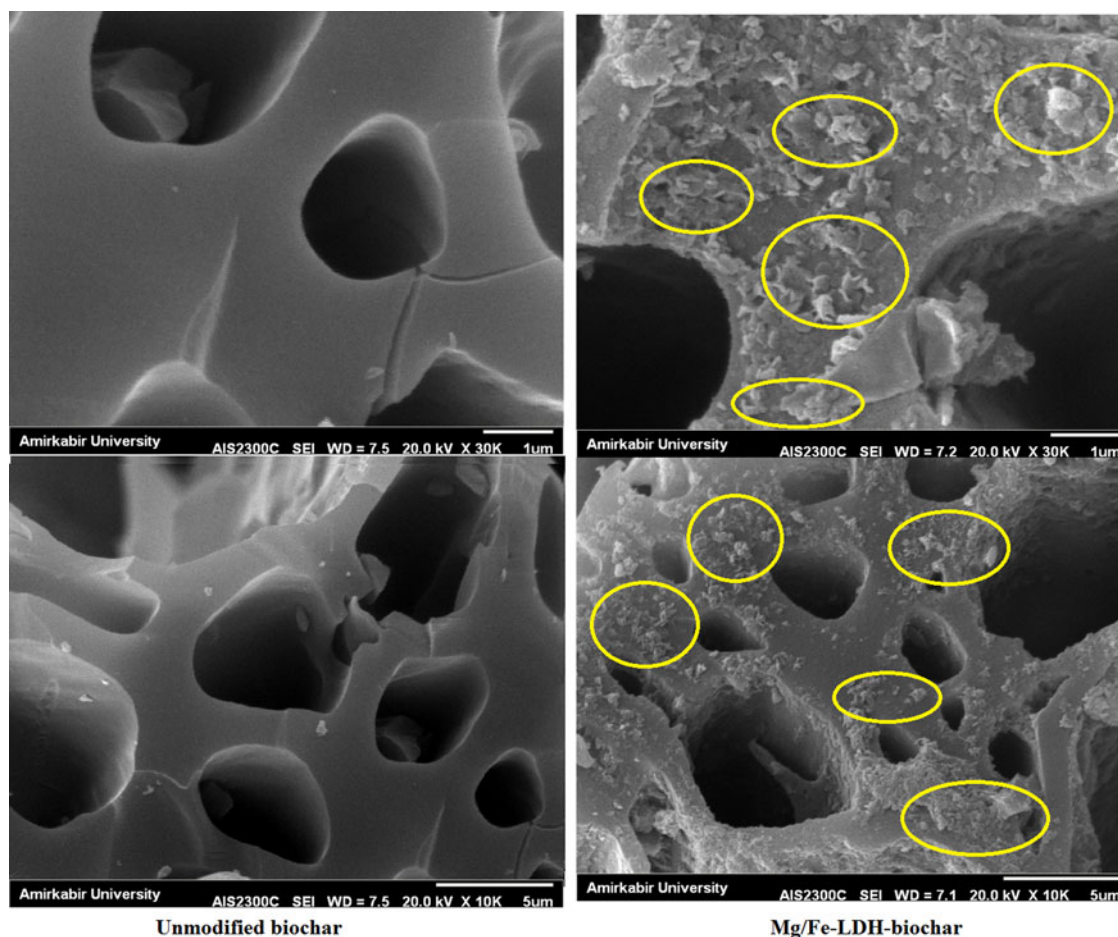


Figure 1 SEM images of unmodified biochar (left) and Magnesium/Iron-Layered Double Hydroxide (Mg/Fe-LDH)-biochar (right). The yellow circles show the locations where Mg/Fe-LDH particles precipitated on biochar.

with the surface functional groups controlled arsenate adsorption on non-modified biochar, which was supported by a shift in the Fourier-transform infrared spectral peaks of biochar surface functional groups such as carboxyl, hydroxyl, and alcohols.

The enhanced adsorption capacity of Mg/Fe-LDH-biochar might be due to the interlayer anion exchange and surface

adsorption on LDH (Goh *et al.* 2008) that coated the porous structure of biochar. Ookubo *et al.* (1993) indicated that the major mechanism for phosphate adsorption using hydroxylated minerals was the displacement of chloride (as interlayer anion) by phosphate. In addition, LDHs have a variable (pH-dependent) charge based on deprotonation and

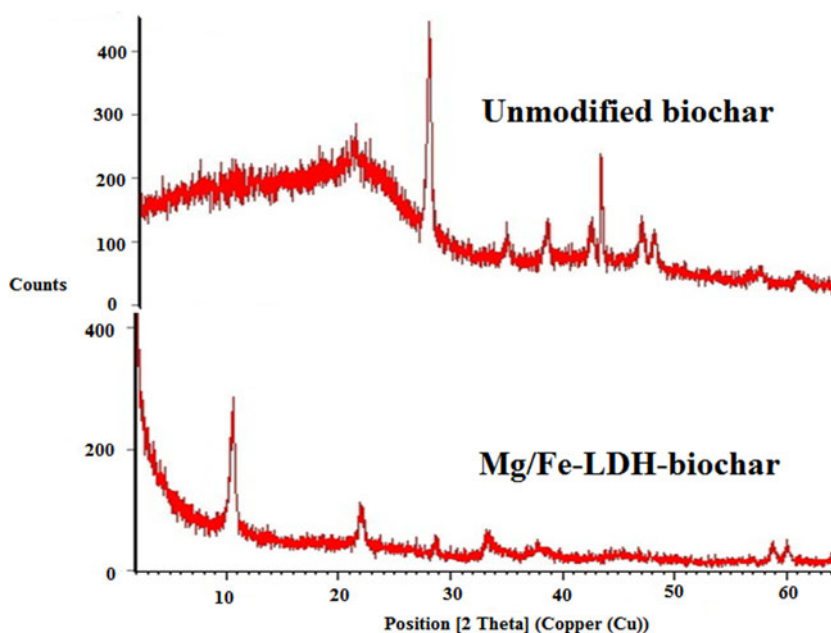


Figure 2 XRD diffractogram of unmodified biochar and Mg/Fe-LDH-biochar.

Table 1 The arsenate removal efficiency by unmodified biochar and Magnesium/Iron-Layered Double Hydroxide (Mg/Fe-LDH)-biochar (pH = 7, ionic strength = 0.01 mol L⁻¹, adsorbent weight = 30 mg, solution volume = 40 mL, contact time = 16 h).

| Arsenate initial concentration (mg L ⁻¹) | Removal efficiency (%) | |
|--|------------------------|-------------------|
| | Unmodified biochar | Mg/Fe-LDH-biochar |
| 0.96 | 4.2 | 54.2 |
| 3.47 | 2.2 | 38.5 |
| 7.33 | 1.3 | 28.5 |
| 9.95 | 1.3 | 22.5 |
| 12.49 | 1.1 | 17.5 |
| 15.52 | 1.2 | 15.6 |
| 19.20 | 0.9 | 12.1 |
| 25.00 | 0.7 | 9.7 |

protonation of surface metal-OH groups. The pHPzc of the Mg/Fe-LDH-biochar in this study was *c.*10 (Section 2.2); hence, when solution initial pH was <10, Mg/Fe-LDH-biochar was positively charged and bound arsenate anions.

2.4. Adsorption kinetics

Kinetics are used to assess the rate-controlling steps and the mechanisms of adsorption. Hence, kinetics are one of the most important factors in designing the adsorption systems for water decontamination. The time-course plots of arsenate adsorption by biochar and Mg/Fe-LDH-biochar are shown in Figure 3. The adsorption of arsenate onto both sorbents increased with contact time. The arsenate adsorption capacity of unmodified biochar reached apparent equilibrium after 240 min. Biochar loaded with Mg/Fe-LDH had a shorter equilibrium time, with more than 90% of the arsenate adsorption by Mg/Fe-LDH-biochar occurring in the first 120 min. After this time, the adsorption rate levelled off (no significant change in arsenate adsorption curve). The fast initial adsorption might have been due to many accessible sites for adsorption on the surface of adsorbents. These findings are comparable with previous results of arsenate adsorption on spherical polymer beads coated with magnesium–aluminium (Mg–Al) and Mg–Fe LDHs, with the time to reach equilibrium reported as 480 min (Nhat Ha *et al.* 2016). Given that pollutant adsorption showed fast kinetics and relatively short time to achieve equilibrium, the adsorbent had a strong capacity for water detoxification in a column system (Zhang *et al.* 2013a, b).

To find out an appropriate kinetic model to describe the process of adsorption, the arsenate adsorption kinetics data were analysed using four models (PFO, PSO, fractional power, and the Elovich). The high value of *R*² and low SE (Table 2) for

the PSO suggested this model described the kinetics of arsenate adsorption on Mg/Fe-LDH-biochar better than the other models. For the PSO model, the adsorption kinetics are controlled by both adsorbent capacity and pollutant concentration (Chaudhry *et al.* 2017); moreover, an electrostatic reaction between pollutant and adsorbent is possible.

Usually, electrostatic adsorption is very rapid (seconds) (Ren *et al.* 2011), and intra-particle diffusion can be a dominant mechanism controlling the adsorption rate. Dispersion of Mg/Fe-LDH particles in the porous structure of biochar (Fig. 1) could have a positive impact on arsenate reaction with the adsorption sites. During the adsorption process, the arsenate molecules were likely first translocated from bulk solution to the LDH surface, and then intra-particle diffusion occurred. Based on the Elovich model parameters values, Mg/Fe-LDH-biochar had faster initial adsorption kinetics ($\alpha = 0.71 \text{ mg g}^{-1} \text{ min}^{-1}$) and lower desorption constants ($\beta = 2.06 \text{ g mg}^{-1}$) than biochar. These findings showed that, in comparison to the non-modified biochar, the LDH-modified biochar had greater affinity for the arsenate ions in solution.

2.5. Adsorption isotherms

Isotherms are key to assessing the adsorption performance and behaviour of adsorbents. As depicted in Figure 4, the arsenate adsorption isotherms for both biochar and Mg/Fe-LDH-biochar showed higher affinity of adsorbents for arsenate present at low than high concentrations. This could be attributed to the lesser number of adsorption active sites compared to arsenate concentration in the solution.

Langmuir, Freundlich, Temkin, and D–R models were employed to predict the capacity and behaviour of arsenate sorption from solution using adsorbents. The results (Table 3; Fig. 4) showed that experimentally measured adsorption was simulated better by the Langmuir and Temkin models than the Freundlich and D–R models for the Mg/Fe-LDH-biochar. Based on the *R*² and SE values (Table 3), the arsenate adsorption onto non-modified biochar is more in line with the Langmuir and Freundlich models. The maximum adsorption capacity (*q*_{max}, Langmuir equation) was calculated to be 3.6 mg arsenate per g of Mg/Fe-LDH-biochar, which was about an order of magnitude higher than that of original biochar (0.35 mg g⁻¹). The Langmuir arsenate adsorption capacity for Mg/Fe-LDH-biochar was greater than that of some reported modified biochars and LDH-containing composites, as summarised in Table 4, but lower than the 25.6 mg g⁻¹ for pure Copper (Cu)–Mg–Fe–Lanthanum-LDH reported by Guo *et al.* (2012) and 24 mg g⁻¹ for lithium-aluminium-based LDH reported by Liu *et al.* (2006). However, the powdered LDHs cannot be used directly in column systems due to the high-

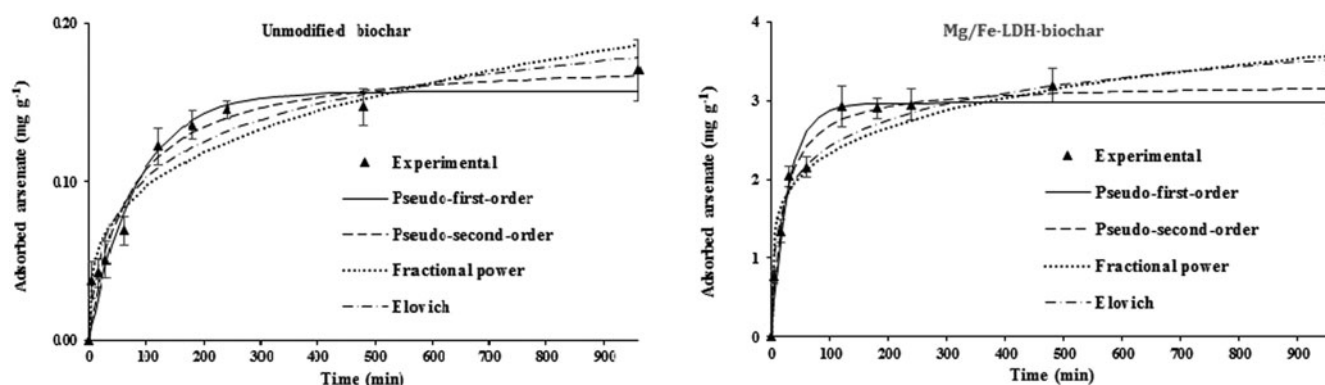


Figure 3 Time-course plots of kinetic models vs measured results of arsenate adsorption on unmodified biochar and Mg/Fe-LDH-biochar (pH = 7, ionic strength = 0.01 mol L⁻¹, adsorbent weight = 30 mg, solution volume = 40 mL). Bars denote \pm standard errors of the means.

Table 2 Kinetic model parameters for arsenate adsorption on unmodified biochar and Mg/Fe-LDH-biochar (pH = 7, ionic strength = 0.01 mol L⁻¹, arsenate concentration = 10 mg L⁻¹, adsorbent weight = 30 mg, solution volume = 40 mL).

| Kinetics model | Adsorbent | Parameters | | | |
|------------------|--------------------------------------|--|-------------------------------|-------|-------|
| | | K_1 (min ⁻¹) | q_e (mg g ⁻¹) | R^2 | SE |
| PFO | Unmodified biochar Mg/Fe-LDH-biochar | 0.01 | 0.16 | 0.96 | 0.015 |
| | | 0.04 | 2.97 | 0.97 | 0.23 |
| PSO | Unmodified biochar Mg/Fe-LDH-biochar | K_2 (g mg ⁻¹ min ⁻¹) | q_e (mg g ⁻¹) | R^2 | SE |
| | | 0.09 | 0.18 | 0.96 | 0.013 |
| | | 0.02 | 3.22 | 0.98 | 0.14 |
| | | K_{FP} (mg g ⁻¹) | v (min ⁻¹) | R^2 | SE |
| Fractional power | Unmodified biochar Mg/Fe-LDH-biochar | 0.03 | 0.29 | 0.92 | 0.018 |
| | | 0.98 | 0.19 | 0.89 | 0.40 |
| Elovich | Unmodified biochar Mg/Fe-LDH-biochar | α (mg g ⁻¹ min ⁻¹) | β (g mg ⁻¹) | R^2 | SE |
| | | 0.006 | 29.16 | 0.95 | 0.014 |
| | | 0.71 | 2.06 | 0.94 | 0.28 |

pressure drop and filtration difficulty resulting from the tight layer stacking. Hence, biochar-supported LDH can be used as effective adsorbent to eliminate arsenate from water in fixed-bed systems.

Increased adsorption capacities of modified biochars compared with unaltered biochars have been reported by other researchers also. Based on He *et al.* (2018), modification of biochar using iron salt (20% w/w Fe) improved the maximum arsenate adsorption capacity 400 times compared with the unaltered biochar. In comparison to the raw pinewood-derived biochar, natural hematite (γ -Fe₂O₃)-modified biochar doubled the capacity for arsenate sorption from the aqueous solutions (Wang *et al.* 2015).

The separation factor (R_L), as a dimensionless parameter, was calculated using the constant of Langmuir (K_L), and the initial concentration of adsorbate in solution (C_0 : mg L⁻¹), with $0 < R_L < 1$ suggesting favourable adsorption (Foo & Hameed 2010). The R_L is calculated from Eq. 15:

$$R_L = \frac{1}{1 + K_L C_0} \quad (15)$$

R_L values of 0.28–0.91 and 0.07–0.67 were calculated for the arsenate adsorption on biochar and Mg/Fe-LDH-biochar in the present study, respectively, which affirmed the favourable process of arsenate adsorption on these two adsorbents. These findings were consistent with Elwakeel & Guibal's (2015) results on the adsorption affinity of arsenate on chitosan modified by Cu(OH)₂ and CuO.

The adsorption apparent energy, E (kJ mol⁻¹), is the energy amount required for transferring a mole of arsenate from the

solution to the surface of adsorbent; it can be calculated using K_{DR} (Eq. 16):

$$E = \frac{1}{\sqrt{2k_{DR}}} \quad (16)$$

In the current study, the average apparent energy (E) values were found to be 0.392 and 1.95 kJ mol⁻¹ for biochar and Mg/Fe-LDH-biochar, respectively. Values of $E < 8.0$ kJ mol⁻¹ have been shown to indicate arsenate adsorption by adsorbents as the physical process at the tested temperature (Chaudhry *et al.* 2017).

2.6. Initial pH effect

The pH is the most important factor in optimising the adsorption systems. Under acidic conditions, arsenate RE in the present study was increased with an increment in the initial solution pH and attained its peak at pH 6, whereas the opposite trend was obvious at the alkaline range for Mg/Fe-LDH-biochar (Fig. 5). The dominant species of arsenate were likely to be Arsenic acid at pH < 2.5, H₂AsO₄⁻ at 2.5 < pH < 7, and HAsO₄²⁻ at pH > 7 (supplementary Fig. 2). This pH dependency of arsenate adsorption has been reported previously for different adsorbents, including Al-enriched biochar (Ding *et al.* 2018), Fe–Zr binary oxide (Ren *et al.* 2011) and Fe-impregnated biochar (He *et al.* 2018).

The solution pH influences the charges on a sorbent by ionisation of the polar functional groups on the surface as well as by arsenate speciation. The common mechanisms suppressing arsenate adsorption at high pHs are (1) the electrostatic repulsion between anionic pollutants (HAsO₄²⁻) and de-protonated surface

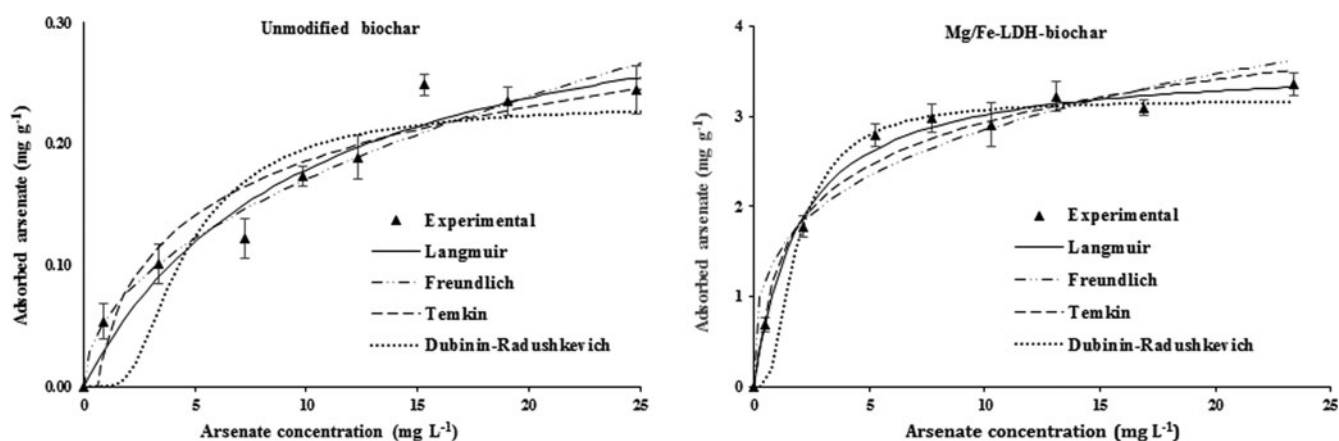
**Figure 4** Isotherm models vs measured results of arsenate adsorption on unmodified biochar and Mg/Fe-LDH-biochar (pH = 7, ionic strength = 0.01 mol L⁻¹, adsorbent weight = 30 mg, solution volume = 40 mL, contact time = 16 h). Bars denote \pm standard errors of the means.

Table 3 The parameters of isotherm models for adsorption of arsenate on unmodified biochar and Mg/Fe-LDH-biochar (pH = 7, ionic strength = 0.01 mol L⁻¹, adsorbent weight = 30 mg, solution volume = 40 mL, contact time = 16 h).

| Isotherm model | Adsorbent | Parameters | | | |
|----------------------|--------------------------------------|---------------------------------------|---|-------|-------|
| | | K_L (L mg ⁻¹) | q_{max} (mg g ⁻¹) | R^2 | SE |
| Langmuir | Unmodified biochar Mg/Fe-LDH-biochar | 0.10 | 0.35 | 0.96 | 0.019 |
| | | 0.52 | 3.60 | 0.99 | 0.11 |
| Freundlich | Unmodified biochar Mg/Fe-LDH-biochar | $K_F [(mg g^{-1})(L mg^{-1})^{-1/n}]$ | $1/n$ | R^2 | SE |
| | | 0.06 | 0.48 | 0.96 | 0.022 |
| | | 1.48 | 0.28 | 0.97 | 0.31 |
| | | b_T (J mol ⁻¹) | A_T (L g ⁻¹) | R^2 | SE |
| Temkin | Unmodified biochar Mg/Fe-LDH-biochar | 37,515 | 1.77 | 0.93 | 0.024 |
| | | 3540.39 | 7.24 | 0.98 | 0.18 |
| Dubinin–Radushkevich | Unmodified biochar Mg/Fe-LDH-biochar | q_s (mg g ⁻¹) | K_{DR} (mol ² kJ ⁻²) | R^2 | SE |
| | | 0.23 | 3.25 | 0.89 | 0.035 |
| | | 3.18 | 0.66 | 0.96 | 0.27 |

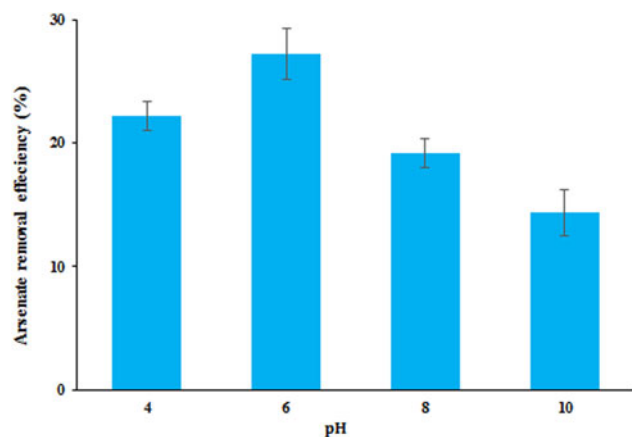
of adsorbent, and (2) the elevated concentration of OH⁻ ions in the aqueous medium (Dias & Fontes 2020).

In general, the oxyanion adsorption on LDHs is affected by the solution pH and commonly is suppressed by an increase in pH (Goh *et al.* 2008). On the other hand, acidic hydrolysis has been shown to lead to dissolution of LDH-containing composites at lower pH values, decreasing their adsorption capacity (Zubair *et al.* 2017). He *et al.* (2018) also reported that by impregnating biochar with Fe, the RE of arsenate increased from 53% to 86% as pH rose from 2 to 6, but it decreased from 83% to 71% as initial pH of the solution increased from 6 to 10.

2.7. IS effect

The IS of contaminant solution affects metal(loid) removal by changing the electrostatic force interactions between adsorbate and adsorbent surface. The results of the arsenate adsorption on the Mg/Fe-LDH-biochar as influenced by the background solution (NaNO₃) IS are shown in supplementary Figure 3. At the solution pH of 7, arsenate RE declined from 21.3% to 11.5% as the NaNO₃ concentration increased from 0.01 to 0.2 mol L⁻¹.

When the electrostatic forces influenced the interactions between pollutants and adsorbents, changing the IS of the background solution could affect the pollutant removal capacity due to pollutant adsorption on the adsorbent being suppressed as the IS increased. The aggregation of the Mg/Fe-LDH-biochar composite due to electrical dual-layer compression (Joseph *et al.*

**Figure 5** Effect of pH on arsenate adsorption on Mg/Fe-LDH-biochar (ionic strength = 0.01 mol L⁻¹, arsenate concentration = 10 mg L⁻¹, adsorbent weight = 30 mg, solution volume = 40 mL, contact time = 16 h). Bars denote ± standard errors of the means.

2019) and a competitive effect of nitrate (as background electrolyte) with an increase in IS are the likely mechanisms governing suppression of arsenate adsorption.

Nitrate could compete for the sorption sites on LDH covering the biochar surface. Indeed, Fe-based LDHs (Sasai *et al.* 2012) and Fe–Mg-LDH/biochar combination (Xue *et al.* 2016) have been used to remove nitrate from solution. The maximum adsorption capacity of nitrate was found to be 24.8 mg g⁻¹ for the biochar modified by Mg–Fe-LDH (Xue *et al.* 2016). In addition, Halajnia *et al.* (2012) showed that Mg–Fe and Mg–Al LDHs have remarkable selectivity for nitrate in complex systems such as simulated soil solution in the presence of sulphate, bicarbonate, and phosphate anions.

2.8. RSM optimisation

The RSM is used for modelling the processes in experiments and is based on regression analysis to minimise the residual variation. In this study, two selected experimental parameters (pH and IS) were optimised by RSM as independent variables (arsenate adsorption on Mg/Fe-LDH-biochar was a response variable). As shown in supplementary Figure 4, arsenate removal from solution increased with a decrease in background solution IS and decreased with an increase in solution pH. The highest adsorption capacity values occurred at 4.2–5.5 pH range and IS of background solution (NaNO₃) lower than 0.05 mol L⁻¹.

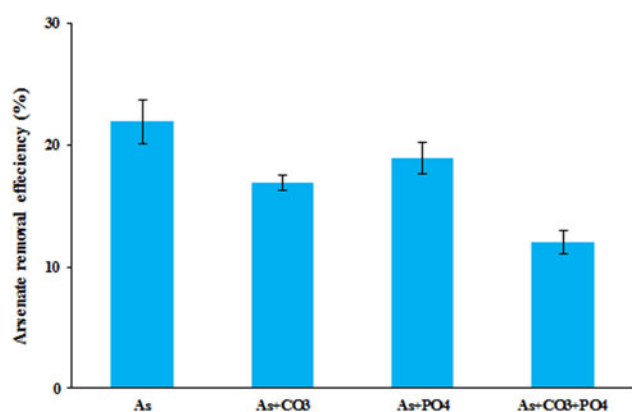
2.9. Co-occurring ions

Carbonate and phosphate are commonly present in a wide range of concentrations in ground/surface water resources, hindering arsenate adsorption on the solid phases. In the present study, competitive adsorption of arsenate, carbonate, and phosphate on Mg/Fe-LDH-biochar decreased arsenate removal (Fig. 6). Arsenate RE when carbonate was present was 16.9%, which was lower than that in arsenate-only solution (21.9%). Xue *et al.* (2016) have demonstrated that when chloride was used as the host anion to Fe–Mg-LDH, carbonate easily replaced chloride in the interlayer space due to carbonate small size, and decreased nitrate adsorption by Fe–Mg-LDH-biochar. Phosphate and arsenate are known to compete for the adsorption sites of the solid-phase surface due to the similar chemical properties also (He *et al.* 2018).

In a study using hydrotalcite as an adsorbent, the presence of competing anions decreased the adsorption of arsenate from solution in the order of carbonate > phosphate > sulphate > chloride (Kiso *et al.* 2005). Gasser *et al.* (2008) observed the high affinity of Mg–Fe-LDH for adsorbing carbonate. The presence of HCO₃⁻ in solution significantly decreased nitrate adsorption on Fe–Mg-LDH-biochar; this effect was greater than the one caused by HPO₄²⁻ and SO₄²⁻ (Xue *et al.* 2016).

Table 4 Comparison of maximum adsorption capacities of some LDH and biochar hybrids that are used as arsenate adsorbents.

| Adsorbent | Adsorption capacities (mg g ⁻¹) | References |
|----------------------------------|---|--------------------------------|
| Magnetic biochar | 3.15 | Zhang <i>et al.</i> (2013b, b) |
| Iron-impregnated biochar | 2.16 | Hu <i>et al.</i> (2015) |
| Hematite-modified biochar | 0.43 | Wang <i>et al.</i> (2015) |
| Al/Mg-LDH | 6.13 | Yang <i>et al.</i> (2006) |
| Mg/Fe-based hydrotalcite | 2.64 | Türk <i>et al.</i> (2009) |
| Ni/Fe-LDH-modified biochar | 4.38 | Wang <i>et al.</i> (2016) |
| Fe/Mg-LDH-modified polymer beads | 1.64 | Nhat <i>et al.</i> (2016) |
| Al/Mg-LDH-modified polymer beads | 1.73 | Nhat <i>et al.</i> (2016) |
| Mg/Fe-LDH-modified biochar | 3.60 | This study |

**Figure 6** Effects of co-occurring (carbonate and phosphate) anions on arsenate adsorption on Mg/Fe-LDH-biochar (pH = 7, adsorbent weight = 30 mg, solution volume = 40 mL, contact time = 16 h). Bars denote \pm standard errors of the means.

2.10. Regeneration cycles of Mg/Fe-LDH-biochar

Adsorbent reusability is one of the most important factors in their safe disposal and further application. To assess the regeneration capacity of Mg/Fe-LDH-biochar in arsenate removal, five consecutive adsorption–desorption cycles were performed (supplementary Fig. 5). A decrease of 20% in arsenate adsorption on Mg/Fe-LDH-biochar was observed over the five adsorption–desorption cycles, which is comparable with the results of regeneration of magnetite biochar/Mg–Al-LDHs by 0.1 mol L⁻¹ NaOH (a decrease of 51% of phosphate adsorption capacity occurred over five cycles of recovery) (Cui *et al.* 2019).

In the present study, 95% of arsenate adsorbed on Mg/Fe-LDH-biochar was released by the 0.1 mol L⁻¹ NaOH desorbing agent. By comparison, it was reported that 0.1 mol L⁻¹ NaOH released 72% of arsenate initially adsorbed on Fe-impregnated biochar (He *et al.* 2018), and 1 mol L⁻¹ potassium phosphate released 70% of arsenate previously adsorbed on Fe₃O₄ nanoparticle-covered biochar (Alchouron *et al.* 2020). A slow decline in the re-adsorption of pollutants by adsorbents with every consecutive adsorption–desorption cycle was attributed to the surface area decrease as well as partial saturation of adsorption sites on the surface of adsorbent (Shakya & Agarwal 2019). Our findings indicate that Mg/Fe-LDH-biochar could be used several times for arsenate adsorption from (and thus decontamination of) aqueous solutions, which would be favourable for home-use water purification, especially in developing regions.

3. Conclusions

Arsenate removal using Mg/Fe-LDH-modified biochar prepared by the co-precipitation method was assessed in this work. The XRD analysis affirmed the presence of LDH minerals in the synthesised composite structure of modified biochar.

Mg/Fe-LDH-biochar showed a good capacity to adsorb arsenate from aqueous media, with the Langmuir q_{max} of 3.6 mg g⁻¹, which was significantly higher than that of non-modified biochar (0.35 mg g⁻¹), and had higher arsenate removal capacity (54.2%; initial concentration \approx 1 mg L⁻¹) than the non-modified biochar (4.2%). Arsenate removal by Mg/Fe-LDH-biochar was significantly affected by pH between 4 and 10; the RE was found to be maximum at pH 6. Moreover, the increases in solution IS and the presence of competing ions (carbonate and phosphate) decreased arsenate adsorption on Mg/Fe-LDH-biochar. Spent Mg/Fe-LDH-biochar (with arsenate adsorbed) could be regenerated by alkaline solution (0.1 mol L⁻¹ NaOH) and reused for at least five times in adsorption–desorption cycles. The results suggest that our simple method of synthesising Mg/Fe-LDH-biochar has potential applications as a non-toxic adsorbent for decontamination of arsenate-polluted water.

4. Supplementary material

Supplementary material is available online at <https://doi.org/10.1017/S1755691022000019>.

5. Acknowledgements

The authors would like to thank Urmia University for equipping the soil chemistry laboratory and the Iran National Science Foundation for financial support (grant number 97024839).

6. References

- Alchouron, J., Navarathna, C., Chludil, H. D., Dewage, N. B., Perez, F., Hassan, E. B., Pittman, C. U., Vega, A. S. & Mlsna, T. E. 2020. Assessing South American *Guadua chacoensis* bamboo biochar and Fe₃O₄ nanoparticle dispersed analogues for aqueous arsenic (V) remediation. *Science of the Total Environment* **706**, 135943.
- Chaudhry, S. A., Khan, T. A. & Ali, I. 2017. Zirconium oxide-coated sand based batch and column adsorptive removal of arsenic from water: isotherm, kinetic and thermodynamic studies. *Egyptian Journal of Petroleum* **26**, 553–63.
- Chaukura, N., Murimba, E. C. & Gwenzi, W. 2017. Sorptive removal of methylene blue from simulated wastewater using biochars derived from pulp and paper sludge. *Environmental Technology and Innovation* **8**, 132–40.
- Cui, Q., Jiao, G., Zheng, J., Wang, T., Wu, G. & Li, G. 2019. Synthesis of a novel magnetic: *Caragana korshinskii* biochar/Mg–Al layered double hydroxide composite and its strong adsorption of phosphate in aqueous solutions. *RSC Advances* **9**, 18641–51.
- Dias, A. C. & Fontes, M. P. F. 2020. Arsenic (V) removal from water using hydrotalcites as adsorbents: a critical review. *Applied Clay Science* **191**, 105615.
- Ding, Z., Xu, X., Phan, T., Hu, X. & Nie, G. 2018. High adsorption performance for As(III) and As(V) onto novel aluminum-enriched biochar derived from abandoned Tetra Paks. *Chemosphere* **208**, 800–07.
- Elwakeel, K. Z. & Guibal, E. 2015. Arsenic(V) sorption using chitosan/Cu(OH)₂ and chitosan/CuO composite sorbents. *Carbohydrate Polymers* **134**, 190–204.

- Foo, K. Y. & Hameed, B. H. 2010. Insights into the modeling of adsorption isotherm systems. *Chemical Engineering Journal* **156**, 2–10.
- Gaskin, J. W., Steiner, C., Harris, K., Das, K. C. & Bibens, B. 2008. Effect of low-temperature pyrolysis conditions on biochar for agricultural use. *Transactions of the ASABE* **51**, 2061–69.
- Gasser, M. S., Mohsen, H. T. & Aly, H. F. 2008. Humic acid adsorption onto Mg/Fe layered double hydroxide. *Colloids and Surfaces A: Physicochemical and Engineering Aspects* **331**, 195–201.
- Giménez, J., Martínez, M., de Pablo, J., Rovira, M. & Duro, L. 2007. Arsenic sorption onto natural hematite, magnetite, and goethite. *Journal of Hazardous Materials* **141**, 575–80.
- Goh, K. H., Lim, T. T. & Dong, Z. 2008. Application of layered double hydroxides for removal of oxyanions: a review. *Water Research* **42**, 1343–68.
- Guo, Y., Zhu, Z., Qiu, Y. & Zhao, J. 2012. Adsorption of arsenate on Cu/Mg/Fe/La layered double hydroxide from aqueous solutions. *Journal of Hazardous Materials* **239**, 279–88.
- Halajnia, A., Oustan, S., Najafi, N., Khataee, A. R. & Lakzian, A. 2012. The adsorption characteristics of nitrate on Mg-Fe and Mg-Al layered double hydroxides in a simulated soil solution. *Applied Clay Science* **70**, 28–36.
- He, R., Peng, Z., Lyu, H., Huang, H., Nan, Q. & Tang, J. 2018. Synthesis and characterization of an iron-impregnated biochar for aqueous arsenic removal. *Science of the Total Environment* **612**, 1177–86.
- Hu, X., Ding, Z., Zimmerman, A. R., Wang, S. & Gao, B. 2015. Batch and column sorption of arsenic onto iron-impregnated biochar synthesized through hydrolysis. *Water Research* **68**, 206–16.
- Hudcová, B., Vitková, M., Ouředníček, P. & Komárek, M. 2019. Stability and stabilizing efficiency of Mg-Fe layered double hydroxides and mixed oxides in aqueous solutions and soils with elevated As(V), Pb (II) and Zn(II) contents. *Science of the Total Environment* **648**, 1511–19.
- Inyinbor, A. A., Adekola, F. A. & Olatunji, G. A. 2016. Kinetics, isotherms and thermodynamic modeling of liquid phase adsorption of rhodamine B dye onto *Raphia hookeri* fruit epicarp. *Water Resources and Industry* **15**, 14–27.
- Joseph, L., Jun, B.-M., Flora, J. R. V., Park, C. M. & Yoon, Y. 2019. Removal of heavy metals from water sources in the developing world using low-cost materials. *Chemosphere* **229**, 142–59.
- Karunanayake, A. G., Navarathna, C. M., Gunatilake, S. R., Crowley, M., Anderson, R., Mohan, D., Perez, F., Pittman, Jr., C. U. & Mlsna, T. 2019. Fe₃O₄ nanoparticles dispersed on Douglas fir biochar for phosphate sorption. *ACS Applied Nano Materials* **2**, 3467–79.
- Kiso, Y., Jung, Y. J., Yamada, T., Nagai, M. & Min, K. S. 2005. Removal properties of arsenic compounds with synthetic hydrotalcite compounds. *Water Science and Technology: Water Supply* **5**, 75–81.
- Li, H., Dong, X., da Silva, E. B., de Oliveira, L. M., Chen, Y. & Ma, L. Q. 2017. Mechanisms of metal sorption by biochars: biochar characteristics and modifications. *Chemosphere* **178**, 466–78.
- Lin, L., Qiu, W., Wang, D., Huang, Q., Song, Z. & Chau, H. W. 2017. Arsenic removal in aqueous solution by a novel Fe-Mn modified biochar composite: characterization and mechanism. *Ecotoxicology and Environmental Safety* **144**, 514–21.
- Liu, Y. T., Wang, M. K., Chen, T. Y., Chiang, P. N., Huang, P. M. & Lee, J. F. 2006. Arsenate sorption on lithium/aluminum layered double hydroxide intercalated by chloride and on gibbsite: sorption isotherms, envelopes, and spectroscopic studies. *Environmental Science & Technology* **40**, 7784–89.
- Manirethan, V., Raval, K. & Balakrishnan, R. M. 2020. Adsorptive removal of trivalent and pentavalent arsenic from aqueous solutions using iron and copper impregnated melanin extracted from the marine bacterium *Pseudomonas stutzeri*. *Environmental Pollution* **257**, 113576.
- Meili, L., Lins, P. V., Zanta, C. L. P. S., Soletti, J. I., Ribeiro, L. M. O., Dornelas, C. B., Silva, T. L. & Vieira, M. G. A. 2019. MgAl-LDH/biochar composites for methylene blue removal by adsorption. *Applied Clay Science* **168**, 11–20.
- Nhat Ha, H. N., Kim Phuong, N. T., Boi An, T., Mai Tho, N. T., Ngoc Thang, T., Quang Minh, B. & Van Du, C. 2016. Arsenate removal by layered double hydroxides embedded into spherical polymer beads: batch and column studies. *Journal of Environmental Science and Health – Part A Toxic/Hazardous Substances and Environmental Engineering* **51**, 403–13.
- Niasar, H. S., Li, H., Kasanneni, T. V. R., Ray, M. B. & Xu, C. C. 2016. Surface amination of activated carbon and petroleum coke for the removal of naphthenic acids and treatment of oil sands process-affected water (OSPW). *Chemical Engineering Journal* **293**, 189–99.
- Ookubo, A., Ooi, K. & Hayashi, H. 1993. Preparation and phosphate Ion-exchange properties of a hydrotalcite-like compound. *Langmuir* **9**, 1418–22.
- Ren, Z., Zhang, G. & Paul Chen, J. 2011. Adsorptive removal of arsenic from water by an iron-zirconium binary oxide adsorbent. *Journal of Colloid and Interface Science* **358**, 230–37.
- Sadeghi, F., Nasser, S., Mosaferi, M., Nabizadeh, R., Yunesian, M. & Mesdaghinia, A. 2017. Statistical analysis of arsenic contamination in drinking water in a city of Iran and its modeling using GIS. *Environmental Monitoring and Assessment* **189**, 230.
- Sasai, R., Norimatsu, W. & Matsumoto, Y. 2012. Nitrate-ion-selective exchange ability of layered double hydroxide consisting of Mg II and Fe III. *Journal of Hazardous Materials* **215**, 311–14.
- Sears, G. W. 1956. Determination of specific surface area of colloidal silica by titration with sodium hydroxide. *Analytical Chemistry* **28**, 1981–83.
- Shabbir, Z., Shahid, M., Khalid, S., Khalid, S., Imran, M., Qureshi, M. I. & Niazi, N. K. 2020. Use of agricultural bio-wastes to remove arsenic from contaminated water. *Environmental Geochemistry and Health*, 1–10. doi: 10.1007/s10653-020-00782-1
- Shakya, A. & Agarwal, T. 2019. Removal of Cr(VI) from water using pineapple peel derived biochars: adsorption potential and re-usability assessment. *Journal of Molecular Liquids* **293**, 111497.
- Singh, B., Singh, B. P. & Cowie, A. L. 2010. Characterisation and evaluation of biochars for their application as a soil amendment. *Soil Research* **48**, 516–25.
- Singh, R., Singh, S., Parihar, P., Singh, V. P. & Prasad, S. M. 2015. Arsenic contamination, consequences and remediation techniques: a review. *Ecotoxicology and Environmental Safety* **112**, 247–70.
- Tan, K. L. & Hameed, B. H. 2017. Insight into the adsorption kinetics models for the removal of contaminants from aqueous solutions. *Journal of the Taiwan Institute of Chemical Engineers* **74**, 25–48.
- Türk, T. U. Ğ. B. A., Alp, İ. B. R. A. H. İ. M. & Deveci, H. A. C. I. 2009. Adsorption of As(V) from water using Mg-Fe-based hydrotalcite (FeHT). *Journal of Hazardous Materials* **171**, 665–70.
- Vithanage, M., Herath, I., Joseph, S., Bundschuh, J., Bolan, N., Ok, Y. S., Kirkham, M. B. & Rinklebe, J. 2017. Interaction of arsenic with biochar in soil and water: a critical review. *Carbon* **113**, 219–30.
- Wang, S., Gao, B., Li, Y., Zimmerman, A. R. & Cao, X. 2016. Sorption of arsenic onto Ni/Fe layered double hydroxide (LDH)-biochar composites. *RSC Advances* **6**, 17792–99.
- Wang, S., Gao, B., Zimmerman, A. R., Li, Y., Ma, L., Harris, W. G. & Migliaccio, K. W. 2015. Removal of arsenic by magnetic biochar prepared from pinewood and natural hematite. *Bioresource Technology* **175**, 391–95.
- WHO. 2017. *Guidelines for drinking-water quality*. 4th edn. Geneva, World Health Organisation, 314–18.
- Xue, L., Gao, B., Wan, Y., Fang, J., Wang, S., Li, Y., Muñoz-Carpena, R. & Yang, L. 2016. High efficiency and selectivity of MgFe-LDH modified wheat-straw biochar in the removal of nitrate from aqueous solutions. *Journal of the Taiwan Institute of Chemical Engineers* **63**, 312–17.
- Yang, L., Dadwhal, M., Shahrivari, Z., Ostwal, M., Liu, P. K., Sahimi, M. & Tsotsis, T. T. 2006. Adsorption of arsenic on layered double hydroxides: effect of the particle size. *Industrial & Engineering Chemistry Research* **45**, 4742–51.
- Yoder, J., Galinato, S., Granatstein, D. & Garcia-Pérez, M. 2011. Economic tradeoff between biochar and bio-oil production via pyrolysis. *Biomass and Bioenergy* **35**, 1851–62.
- Zhang, M., Gao, B., Varnosfaderani, S., Hebard, A., Yao, Y. & Inyang, M. 2013a. Preparation and characterization of a novel magnetic biochar for arsenic removal. *Bioresource Technology* **130**, 457–62.
- Zhang, M., Gao, B., Yao, Y. & Inyang, M. 2013b. Phosphate removal ability of biochar/MgAl-LDH ultra-fine composites prepared by liquid-phase deposition. *Chemosphere* **92**, 1042–47.
- Zubair, M., Daud, M., McKay, G., Shehzad, F. & Al-Harthi, M. A. 2017. Recent progress in layered double hydroxides (LDH)-containing hybrids as adsorbents for water remediation. *Applied Clay Science* **143**, 279–92.